ResearchGate

See discussions, stats, and author profiles for this publication at: https://www.researchgate.net/publication/234841634

Determination of hot and cold rolling textures of steels: Combined Bayesian neural network model

Article *in* Materials Science and Technology · March 2012

DOI: 10.1179/1743284711Y.0000000035

CITATIONS
4

READS
156

5 authors, including:

Carlos Capdevila
Centro Nacional de Investigaciones Metalúrgicas (CENIM)
255 PUBLICATIONS **4,543** CITATIONS
SEE PROFILE

Isaac Toda-Caraballo
Centro Nacional de Investigaciones Metalúrgicas (CENIM)
46 PUBLICATIONS **1,049** CITATIONS
SEE PROFILE

Francisca G. Caballero
Spanish National Research Council
288 PUBLICATIONS **9,680** CITATIONS
SEE PROFILE

Carlos Garcia-Mateo
Centro Nacional de Investigaciones Metalúrgicas (CENIM)
206 PUBLICATIONS **6,725** CITATIONS
SEE PROFILE

Some of the authors of this publication are also working on these related projects:

Guest Editor for Applied Sciences : Special Issue in Microstructural characterization of metals, from Nano to Macro scale View project

New Bainitis Steels View project

All content following this page was uploaded by Carlos García de Andrés on 04 June 2014.

The user has requested enhancement of the downloaded file.

Determination of hot and cold rolling textures of steels: combined Bayesian neural network model

C. Capdevila*, I. Toda, F. G. Caballero, C. Garcia-Mateo and C. G. de Andres

The work reported in the present paper outlines the use of a combined artificial neural network model capable of fast online prediction of textures in low and extralow carbon steels. We approach the problem by a Bayesian framework neural network model that takes into account as input to the model the influence of 23 parameters describing the chemical composition and the thermomechanical processes, such as austenite and ferrite rolling, coiling, cold working and subsequent annealing, involved in the production route of low and extralow carbon steels. The output of the model is in the form of fibre texture data. The predictions of the network provide an excellent match to the experimentally measured data. The results presented in the present paper demonstrate that this model can help in optimising the normal anisotropy r_m of steel products.

Keywords: Artificial neural network, Texture prediction, Anisotropy, Hot rolling, Cold rolling, Steel

Published by Maney Publishing (c) IOM Communications Ltd

Introduction

In recent years, there has been a steady increase in interest from the automotive industry in isotropic steel products, i.e. steel products with a minimum of variation of mechanical properties, most noticeably drawability, in the plane of the sheet. Therefore, corresponding to the ever increasing demands of the sheet metal forming industry, future generations of drawable steel grades will need to ensure a well balanced equilibrium between drawability on the one hand and drawing anisotropy on the other hand.

Great demands are placed on the quality of deep drawing steels with regard to their surface and mechanical properties. Knowledge of the microstructural and textural evolution in the individual process stages is of the highest importance to improve the sheet quality in terms of its deep drawing properties. In the past, the derivation of models for microstructural and textural evolution was carried out on the basis of the results of laboratory tests using the reverse rolling technique. This applies in particular to the rolling experiments, which can be performed at low rolling speeds only, e.g. $\sim$1 m s^{-1}, and interpass times of $>$5 s.

Nevertheless, the continuously increasing requirements on the quality of flat products demand the further development of both materials and their production technologies. Such development can be achieved in modern continuous hot strip mills that operate with rolling speeds of up to 20 m s^{-1} and interpass times of 0·1 s. From this follows that differences in microstructure and properties existed between strips rolled in the laboratory and in practice, which reveals that laboratory plants and even pilot mills often cannot accurately simulate production conditions.

To close this gap, in the present paper, it was decided to employ an entirely new tool patterned to the human brain, i.e. 'artificial neural networks'. Such networks 'learn' from the massive volume of incoming data and the relationships involved and gain experience from the systematic observation of recurring events. This makes them capable of supporting traditional mathematical models or replacing them entirely. Their learning ability also enables neural networks to adapt continuously to changing process states. The present paper illustrates the use of such modelling technique in the prediction of the texture for low carbon (LC) and extralow carbon (ELC) deep drawing steel qualities as a function of chemistry and thermomechanical processing parameters. The drawing properties of the steel are essentially determined by the texture of the finished product. The model is then used in the prediction of the normal anisotropy ratio, or the r_m value, for LC and ELC steel. The r_m value evaluates the drawability of a sheet material, i.e. its capacity to achieve a high degree of plastic flow in the plane of the sheet while offering sufficient resistance to flow in the thickness direction. On this basis, the present work provides an example of how neural network modelling could be incorporated into the optimisation process of steel sheets and how the rolling processing parameters affect the texture of such steels that satisfy the increasing drawability of advanced steel for automotive applications.

Build of model

The drawing properties of steel are essentially determined by the texture of the finished product.[1] Figure 1 shows the

Materalia Research Group, Department of Physical Metallurgy, Centro Nacional de Investigaciones Metalúrgicas (CENIM), Consejo Superior de Investigaciones Científicas (CSIC), Avda. Gregorio del Amo, 8., Madrid E-28040, Spain

*Corresponding author, email ccm@cenim.csic.es

© 2012 Institute of Materials, Minerals and Mining
Published by Maney on behalf of the Institute
Received 15 February 2011; accepted 5 April 2011
DOI 10.1179/1743284711Y.0000000035

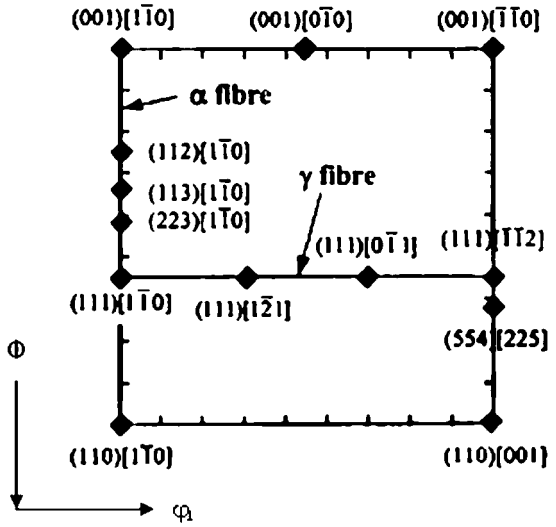

1 Section (φ_2=45°) of Euler space showing ideal bcc rolling and recrystallisation components

φ_2=45° sections of the orientation distribution function, because this section contains all the important rolling and recrystallisation components of a bcc material. The texture components depicted in Fig. 1 can be used as a key to read the texture results obtained by the model. In the figure, it can be seen that the dominant components mainly concentrate along two fibres: α-fibre (RD‖⟨110⟩), with main texture components within the range of {001}⟨110⟩ (ϕ_1=0°, Φ=0°, ϕ_2=45°) to {111}⟨110⟩ (ϕ_1=0°, Φ=55°, ϕ_2=45°), and the γ-fibre (ND‖⟨111⟩), where RD is the rolling direction and ND is the direction parallel to the sheet normal. It is commonly known that, for a bcc material, the γ-fibre ⟨111⟩‖ND texture is the desired texture type to obtain the highest drawability. In consequence, texture control in drawing steel grades consistently aims to develop the highest possible intensity along the y-fibre.

The texture strength has been modelled by determining the α- and γ-fibre intensities [f(g)]. The α-fibre intensity has been calculated for 0°<Φ<90° in steps of Φ=5°. Each step corresponds to an independent neural network model. On the other hand, the γ-fibre has been calculated for 60°<φ_1<90° in steps of φ_1=10°, with independent models for each step. Therefore, 19 different models have been developed to characterise the α-fibre and four models to characterise the γ-fibre.

In this sense, the focus of the present work was the investigation of the influence of rolling parameters on the α- and γ-fibres of hot strip and the derived cold strip from ultralow carbon, interstitial free (IF), LC, high strength low alloyed and ELC steel grades. Figure 2 shows the product flow and the major characteristics of the hot and cold strip mill lines. The following parameters were varied to investigate their effects on strip properties: roughing temperature (RT) and reduction, reheating temperature, finishing temperature (FT) and reduction, rolling speed, cooling conditions, coil temperature and rolls with roll gap lubrication.

The second aim of the present paper is to clarify the impact of the hot strip state on the properties of cold strip. In this sense, parameters such as cold rolling reduction (CRED) and annealing temperature (AT) were systematically analysed and incorporated in the dataset. Likewise, special attention has been paid to the influence of hot rolling on the subsequent cold rolled microstructure. The proposed model allows a more deep understanding of the influence of each parameter of the rolling stand (hot and cold rolling) on the final microstructure of deep drawable steels. Furthermore, this model allows a systematic development of new materials with regard to deep drawing properties depending on the deformation conditions.

Database

The models that constitute the α- and γ-fibres require a complete description of the chemical composition and processing parameters. A literature survey[2–9] allows us to collect 240 individual cases where detailed chemical composition, hot rolling processing parameters, coiling temperature, cold reduction and AT values were reported for each of the 18 individual models that form the α-fibre and the four individual models that form the γ-fibre. The hot rolling data collected correspond to those obtained from pilot mill. The pilot mill comprises four rolling stands so arranged in one line that roughing is possible with one reversing two-high stand followed by continuous finishing with all four stands (reversing two-high plus three continuous two-high stands). Samples are heated in an inductor allowing fast heating to 1350°C. All the stands are equipped with roll gap lubrication, and the interpass times can be varied by modification of the rolling speeds and the distances between stands. The hot rolled samples are then cold rolled and continuously annealed in a radiation furnace simulator.

The variables considered are the following: chemical composition in weight per cent (carbon, manganese, silicon, aluminium, chromium, nitrogen, niobium and titanium), slab reheating temperature (SRT), roughing stage [temperature (RT), speed (RS), passes (nR) and reduction (RRED)], finishing stage [temperature (FT), speed (FS), passes (nF) and reduction (FRED)], the use of lubricant during rolling (LUB: without=0; and lubricant=1), coiling temperature (CT), CRED and finally AT. Table 1 shows the list of 23 input variables used for the α- and γ-fibres analysis, and Table 2 lists the output variables considered.

Brief description of neural network

The aim is to be able to estimate f(g) evolution with Φ for α-fibre and with φ_1 for γ-fibre as a function of the variables listed in Table 1. In the present case, the network was trained using a randomly chosen of 130 examples from a total of 240 available; the remaining 110 examples were used as new experiments to test the trained network. Linear functions of the inputs x_j are operated by a hyperbolic tangent transfer function

$$h_i = \tanh\left[\sum_j w_{ij}^{(1)} x_j + \theta_i^{(1)}\right] \quad (1)$$

so that each input contributes to every hidden unit. The bias is designated $\theta_i^{(1)}$ and is analogous to the constant that appears in linear regression. The strength of the transfer function is in each case determined by the weight $w_{ij}^{(1)}$. The transfer to the output y is linear

$$y = \sum_i w_i^{(2)} h_i + \theta^{(2)} \quad (2)$$

Published by Maney Publishing (c) IOM Communications Ltd

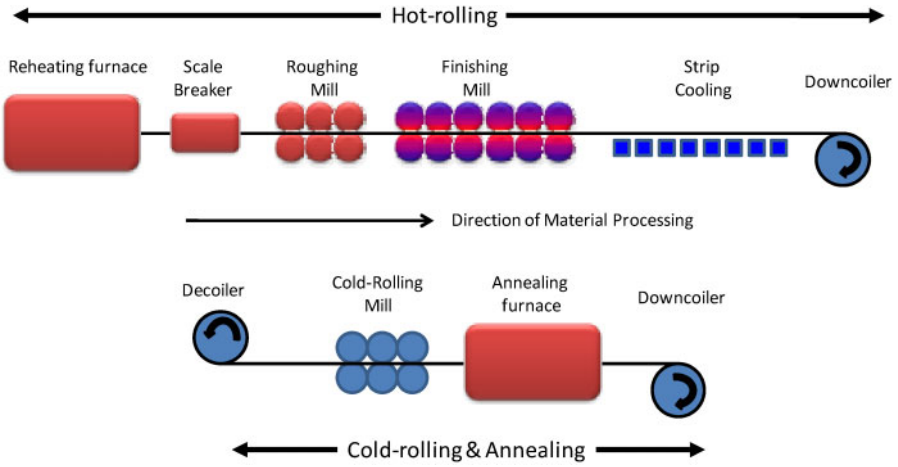

2 Scheme of hot and cold rolling mills for steel production

This specification of the network structure, together with the set of weights, is a complete description of the formula relating the inputs to the output. The weights were determined by training the network, and the details are described by MaKay.[10,11] The training involves a minimisation of the regularised sum of squared errors.

The term σ_v was the framework estimation of the noise level of the data. Figure 3 shows, as an example, the inferred noise level of the $\Phi=45^\circ$ model. It is clear from the figure that the inferred noise level decreases monotonically as the number of hidden units increase. Table 2 lists the σ_v values obtained for each model. However, the complexity of the model also increases with the number of hidden units. To find out the optimum number of hidden units of the model, the following procedure was used. The experimental data were partitioned equally and randomly into a test dataset and a training dataset. Only the latter was used to train the model, whose ability to generalist was examined by checking its performance on the unseen test data. The test error T_{en} is a reflection of the ability of the model to predict in the test data, i.e.

$$T_{en}=0{\cdot}5\sum_{n}(y_n-t_n)^2 \tag{3}$$

where y_n is the set of predictions made by the model, and t_n is the set of target (experimental) values.

A high degree of complexity may not be justified, and in an extreme case, the model may, in a meaningless way, attempt to fit the noise in the experimental data. MaKay[12,13] has made a detailed study of this problem and defined a quantity (the 'evidence') that comments on the probability of a model. In circumstances where two models give similar results for the known data, the more probable model would be predicted to be that which is simpler; this simple model would have a higher value of evidence. The evidence framework was used to control σ_v. The number of hidden units was set by examining the

Table 1 Variables that influence texture: SD is standard deviation

		Min.	Max.	Average	SD
Group 1	C/wt-%	0·0019	0·055	0·0167	0·0196
	Mn/wt-%	0·097	0·25	0·1819	0·0463
	Si/wt-%	0	0·071	0·026	0·0262
	P/wt-%	0·003	0·011	0·007	0·0026
	S/wt-%	0·004	0·013	0·008	0·0026
	Al/wt-%	0·015	0·049	0·0409	0·0082
	Cr/wt-%	0	0·027	0·0203	0·0076
	N/wt-%	0·0018	0·0049	0·0025	0·0008
	Nb/wt-%	0	0·029	0·0121	0·0124
	Ti/wt-%	0	0·041	0·0137	0·0162
Group 2	RT/°C	900	1200	1016·1506	82·3259
	nR	2	7	2·5439	1·1583
	RS/m s^{-1}	0·5	4	1·2109	0·7269
	RRED/%	30	80	38·4161	15·021
	SRT/°C	1050	1250	1155·8996	96·7015
	FT/°C	535	950	837·0167	98·5536
	nF	1	4	3·7908	0·6467
	FS/m s^{-1}	0·5	7	3·2331	1·8317
	FRED/ %	48	98·6	86·3158	6·9489
	LUB	0	1	0·4979	0·501
Group 3	CT/°C	400	730	668·7531	102·413
	CRED/%	0	90	51·6987	38·6548
	AT/°C	20	830	388·9749	365·5413

Table 2 Output variables considered on describing α- and γ-fibres: SD is standard deviation, σv is inferred noise level and $\Phi\#\#$ indicates model corresponding to each 5*P* step in $0P<\Phi<90P$ for α-fibre (in the same sense, $\Phi\#\#$ indicates model corresponding to each 10*P* step in $60P<\Pi_1<90P$ for γ-fibre)

	Min.	Max.	Average	SD	σ_v
Φ0	0	21	6·2731	5·217	0·12592
Φ5	0	22	6·3916	5·2351	0·11728
Φ10	0	24	6·5421	5·2321	0·10535
Φ15	0	24	6·6196	5·0916	0·08901
Φ20	0	24	6·6836	4·9716	0·09034
Φ25	0	24	6·7324	4·9775	0·09668
Φ30	0	23	6·7132	4·9826	0·09731
Φ35	0	22	6·7113	4·9549	0·09499
Φ40	0·5	35	6·6881	4·8271	0·047376
Φ45	0·5	15	6·3453	3·4699	0·080105
Φ50	0	13	6·0516	2·8367	0·10696
Φ55	0	15	5·4109	3·039	0·085474
Φ60	0	14	4·1294	2·6751	0·065997
Φ65	0	10	2·6394	1·8149	0·056186
Φ70	0	25	1·7011	1·8263	0·061479
Φ75	0	3	1·1913	0·6911	0·10554
Φ80	0	10	0·9256	0·8861	0·064904
Φ85	0	3	0·6592	0·6411	0·11
Φ90	0	4	0·6001	0·7078	0·1148
ϕ60	0·5	15	6·0456	2·966	0·056756
ϕ70	0	25	6·2615	1·8263	0·060707
ϕ80	0	22	6·7956	4·1269	0·06085
ϕ90	0	22	7·0367	4·4081	0·066218

Published by Maney Publishing (c) IOM Communications Ltd

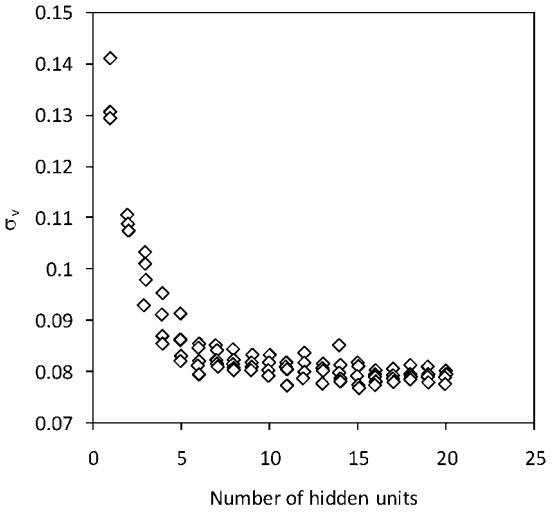

3 Variation in inferred noise level σ_V as function of number of hidden units for Φ=45° model

performance on test data. A combination of Bayesian and pragmatic statistical techniques was therefore used to control the complexity of the model.[14] For the particular case of the Φ=45° model shown in Fig. 3, it could be concluded that a large number of hidden units did not give significantly lower values of σ_v; indeed, 11 hidden units were found to give a reasonable level of complexity to represent the variations of f(g) as a function of the input variables of Table 1.

On the other hand, it is possible that a committee of models can make a more reliable prediction than an individual model. The best models were ranked using the values of their test errors (equation (3)), as Fig. 4*a–d* and *e* presents, for the respective α- and γ-fibres. A committee of models could then be formed by combining the prediction of the best L models, where L=1, 2, …. The size of the committee is therefore given by the value of L.

The combined test error of the predictions made by a committee of L models, ranked 1, 2, …, q, …, L, each with n lines of test data, is calculated in a similar manner to the test error of a single model

$$T_{en} = 0{\cdot}5 \sum_{n} (\overline{y_n} - t_n)^2$$
$$\overline{y}_n = \frac{1}{L} \sum_{q} y_n^{(q)} \qquad (4)$$

where $y_n^{(q)}$ is the set of predictions made by the model, and t_n is the set of target (experimental) values. As Fig. 5 suggests, the combined test error goes through a minimum for the committee made up of a certain number of models, as listed in Table 3. However, there some exceptions such as the one for Φ=75° and ϕ=60° models, where the build of a committee does not reduce the test error. In such cases, the best model is considered only. From a comparison between the results presented in Figs. 4 and 5, a reduction in test error and hence improved predictions using the committee of models approach instead of the best model alone are clear. A comparison between the predicted and measured values of Φ=45° and ϕ=60°, as an example, for the training and test data is shown in Fig. 6 for the best committee of each fibre component.

Nevertheless, the practice of using a best fit function does not adequately describe the uncertainties in regions of the input space where data are spare or noisy. MaKay[12,13] has developed a particularly useful treatment of neural networks in a Bayesian framework, which allows the calculation of error bars representing the uncertainty in the fitting parameters. The method recognises that there are many functions that can be fitted or extrapolated into uncertain regions of the input space without unduly compromising the fit in adjacent regions, which are rich in accurate data. Instead of calculating a unique set of weights, a probability distribution of sets of weights is used to define the fitting uncertainty. The error bars therefore become larger when data are spare or locally noisy.

Figures 7 and 8 illustrate the significance σ_w of each of the input variables, as perceived by the neural network, in influencing the components of α- and γ-fibres respectively. The variables analysed are organised into three groups, i.e. group 1, hot rolling; group 2, chemical composition; and group 3, cold rolling and annealing (*see* Table 1). The value of σ_w is normalised to 100, i.e. the value of σ_w for a specific variable indicates the degree of influence in percentage. The metallurgical significance of the results predicted by the models is discussed below, but a first approximation of the influence of each one of the variables studied could be drawn from a close observation of Figs. 7 and 8.

As a general comment for the 19 models of α-fibre components and the four models of γ-fibre models, it is clear that the AT after cold rolling, together with CRED, clearly has a large intrinsic effect on α-fibre components and in a minor scale on γ-fibre components. In terms of hot rolling processing parameters, the finishing stage has a significantly larger influence than the roughing stage. Particularly, SRT and FT significantly affect the intensity of the α-fibre components for the case of Φ0° to Φ20° components. A relative low influence of those parameters is observed for the remaining components of α-fibre. It is also worth mentioning the lack of influence of *a priori* important variables, such as finishing reduction (FRED), speed of rolling (FS) and number of steps involved in the finishing process (nF).

On the other hand, the finishing and roughing temperatures have a large influence on the components of γ-fibre, which is of technological importance since the intensity of such fibre is closely related to the deep drawing properties of the steels, as it has been thoroughly reported in the literature in the last decade.

Special attention to the role of chemical composition on the f(g) values of α- and γ-fibre components has been paid. The chemical composition is not very relevant for the development of α-fibre components (with the exception of Φ70° component). However, it is important to highlight the spectacular relevance of microalloying elements, such as Nb and Ti, have on the intensity of γ-fibre components. This is consistent with the well reported influence of these microalloying elements on tiding up the interstitial elements, such as C and N, which have a negative influence on the development of good deep drawability properties. This broad idea is consistent with the high influence of C content in γ-fibre components, is it is seen in Fig. 8.

The high influence that the lubricant (LUB) has on the Φ0° component of the α-fibre is surprising, which could

Published by Maney Publishing (c) IOM Communications Ltd

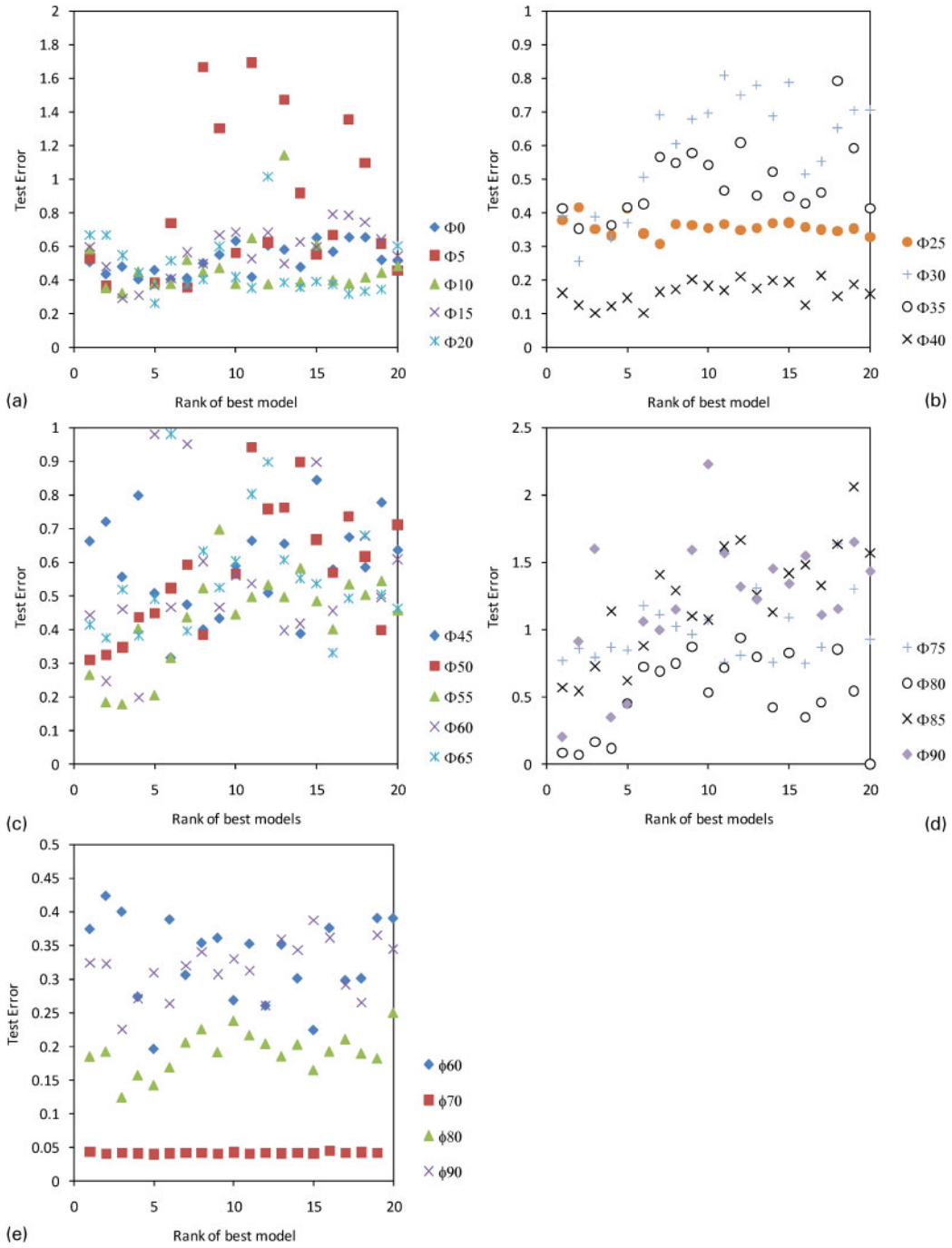

4 Test error values of 20 best models for *a* α-fibre (Φ between 0 and 20°), *b* α-fibre (Φ between 25 and 40°), *c* α-fibre (Φ between 45 and 65°), *d* α-fibre (Φ between 75 and 90°) and *e* γ-fibre models

be related with the role of shear friction during rolling on the development of such component, as it has been reported.[15] On the other hand, this parameter has a rather negligible influence on the remaining α- and γ-fibre components.

Applications of model: evolution of hot rolling texture in IF steels

The effect of rolling parameters, such as SRT, FS and FT, on IF steel is reported in this section (*see* Table 4 for chemical composition). Two situations have been considered: IF steel hot rolled in austenitic (FT=930°C) as well as in the upper (FT=800°C) and lower ferritic region (FT=650°C). For ferritic rolling, high and low reheating temperatures of 1250 and 1050°C have been investigated. Two different rolling speeds in the finishing mill have been considered (0·5 and 7 m s^{-1}).

Figure 9 shows the evolution of both α- and γ-fibres for the two SRTs selected. The FT value considered in the calculations is 930°C, and FS=0·5 m s^{-1}. The remaining rolling parameters considered are listed in Table 4. It is clear from the results presented that the simulations are consistent with the typical low intensities on their α- and γ-fibre expected after hot rolling processing. It could be concluded that there is no significant influence of SRT on the hot rolling texture.

On the other hand, Fig. 10 presents the results for the influence of FT on the hot rolling texture. Three different temperatures have been selected: an FT of 930°C, which

Published by Maney Publishing (c) IOM Communications Ltd

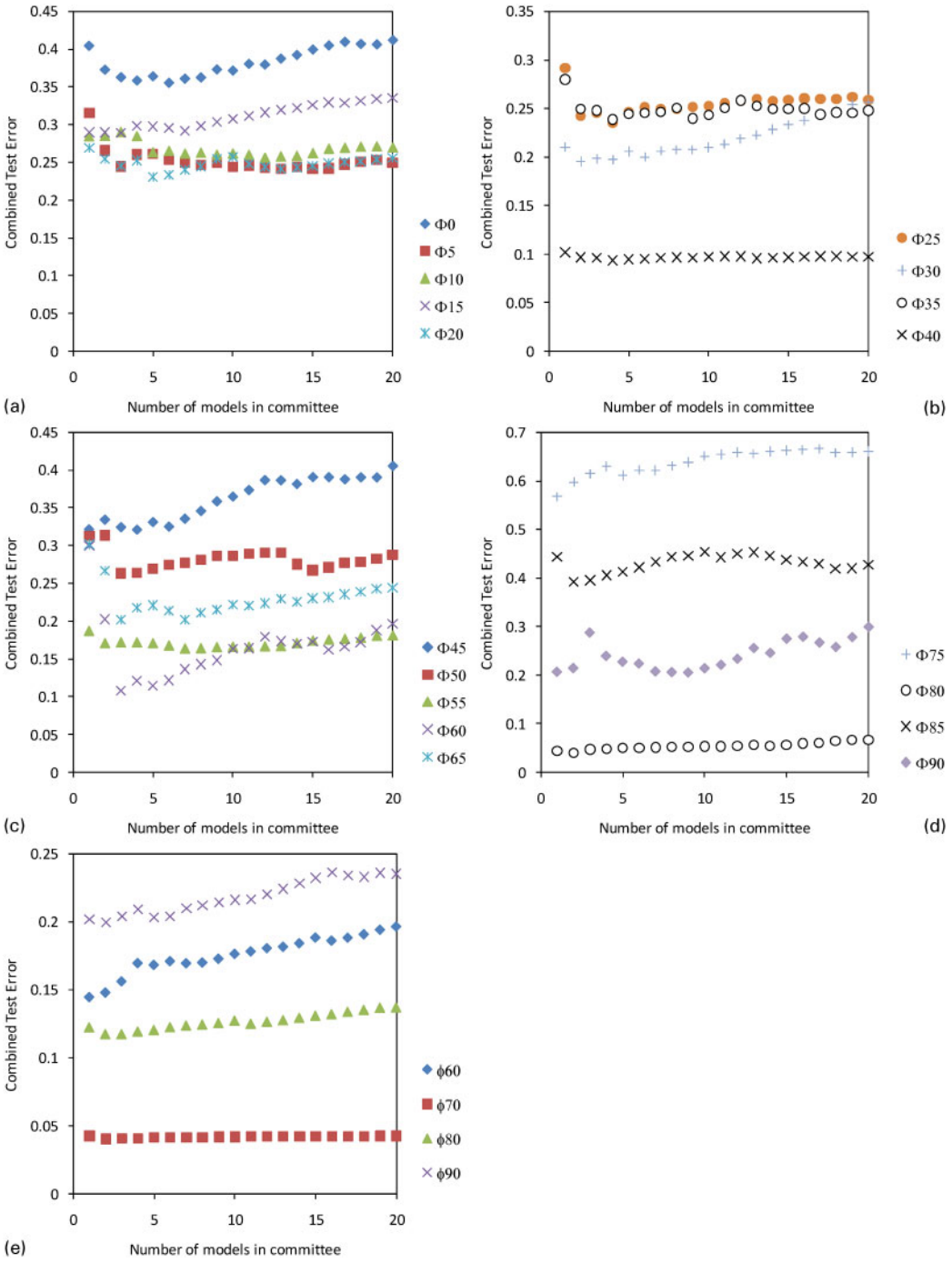

5 Combined test error values of committee for *a* α-fibre (Φ between 0 and 20°), *b* α-fibre (Φ between 25 and 40°), *c* α-fibre (Φ between 45 and 65°), *d* α-fibre (Φ between 75 and 90°) and *e* γ-fibre models

indicates austenitic rolling and subsequent air cooling to room temperature, and FT values of 800 and 650°C for the upper and lower ferrite region with the higher reheating temperature of 1250°C (*see* Table 4 for remaining processing parameters). Compared with austenitic rolling, the intensities are significantly higher for both α- and γ-fibres. Significant differences of the intensities can be observed especially for the α-fibre but also for the γ-fibre with FT in the ferrite region. However, they could not be linked to an influence of rolling parameters, such as SRT, RT and LUB. The attempt to link the differences to the roll speed fails. Figure 11 shows the differences in both α- and γ-fibres with FS for FT=800°C (*see* Table 4 for the remaining parameters).

Applications of model: effect of chemical composition and processing parameters on normal anisotropy index r_m in deep drawability quality (DDQ) steels

On DDQ steel, particular attention to $\{111\}\langle uvw\rangle$ orientation should be paid.[16,17] It has been demonstrated that high r_m values are displayed by materials that have a high proportion of grains oriented with their {111} planes parallel to the sheet plane, i.e. by materials that possess a strong {111} type texture (or γ-fibre texture). Other texture components, such as {001}, have been found to be detrimental to the drawability, and in this sense, and according with the work reported by

Published by Maney Publishing (c) IOM Communications Ltd

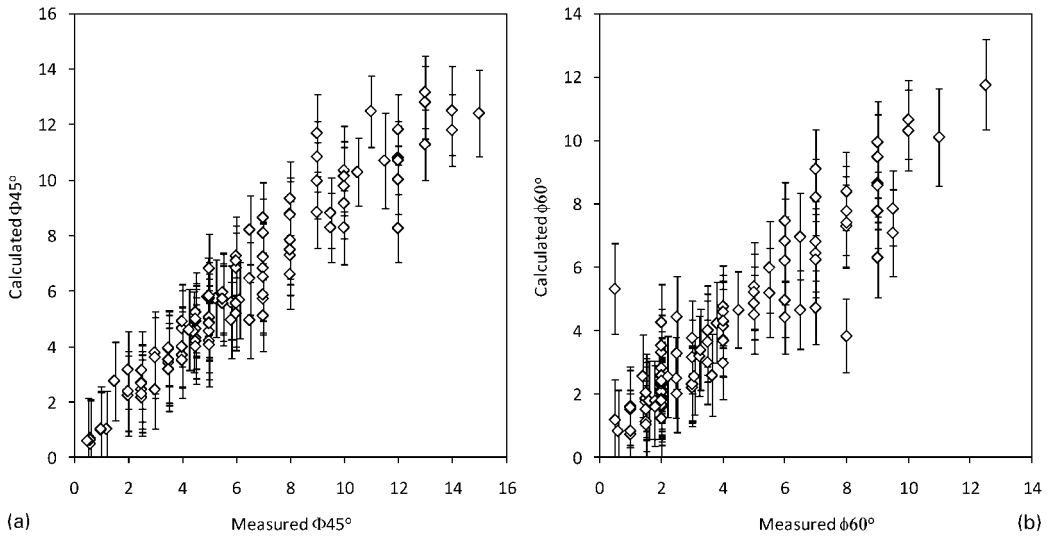

6 Comparison between predicted and measured values of *a* Φ=45° and *b* ϕ=60° using their respective committee of models

Daniel and Jonas,[18] the most desired texture components to obtain good drawability properties are {111}⟨110⟩ and {111}⟨112⟩, and the most undesired ones will be {110}⟨001⟩ and {001}⟨110⟩. In practice, the intensity ratio of the above two components $I(111)/I(100)$ is found to be linearly related to r_m, as it was determined by Held.[19] Held measured the evolution of r_m with α- and γ-fibre intensity ratios and concluded that there is a linear

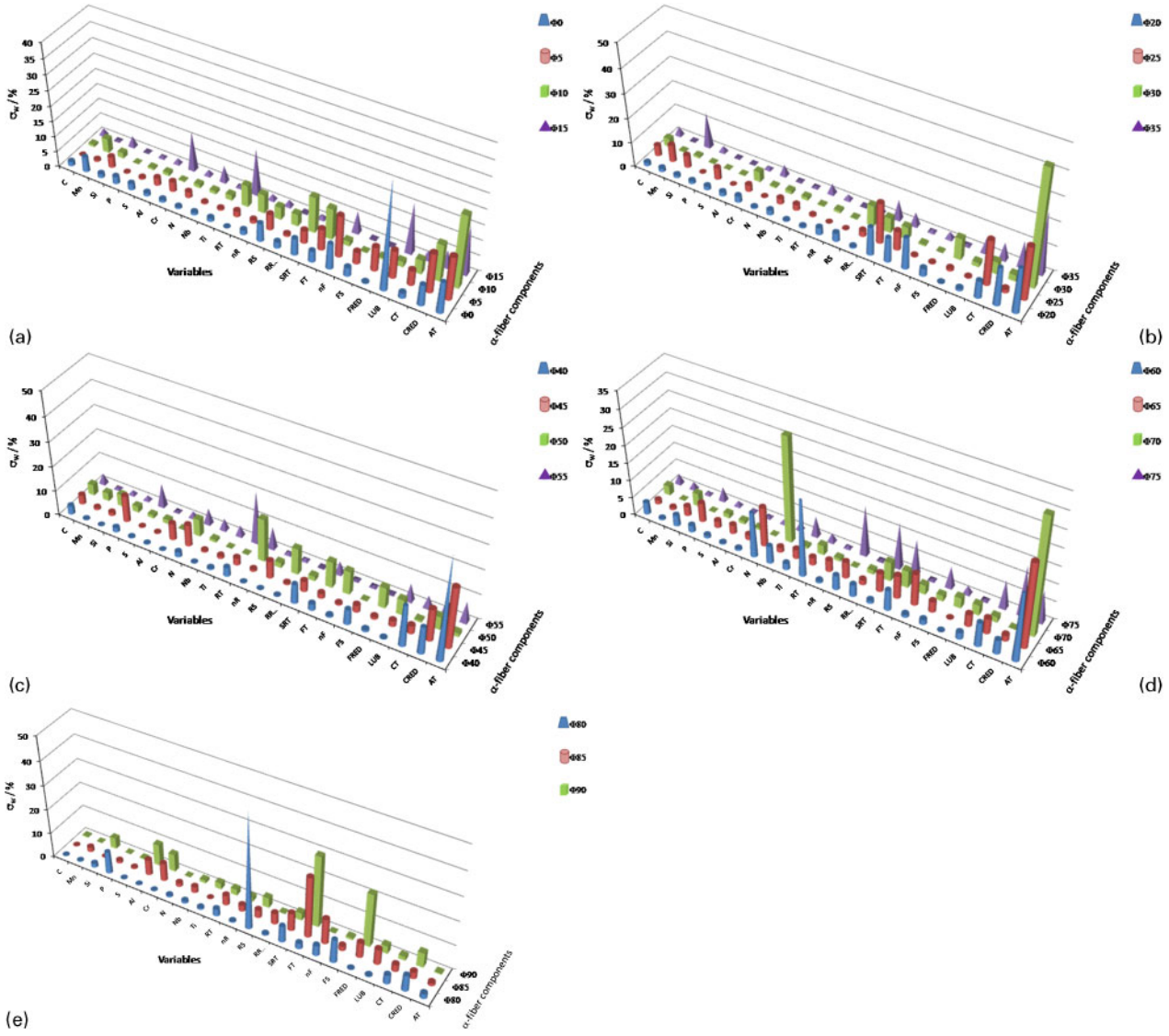

7 Histogram showing significance of input variables in influencing α-fibre components perceived by their respective best models

Published by Maney Publishing (c) IOM Communications Ltd

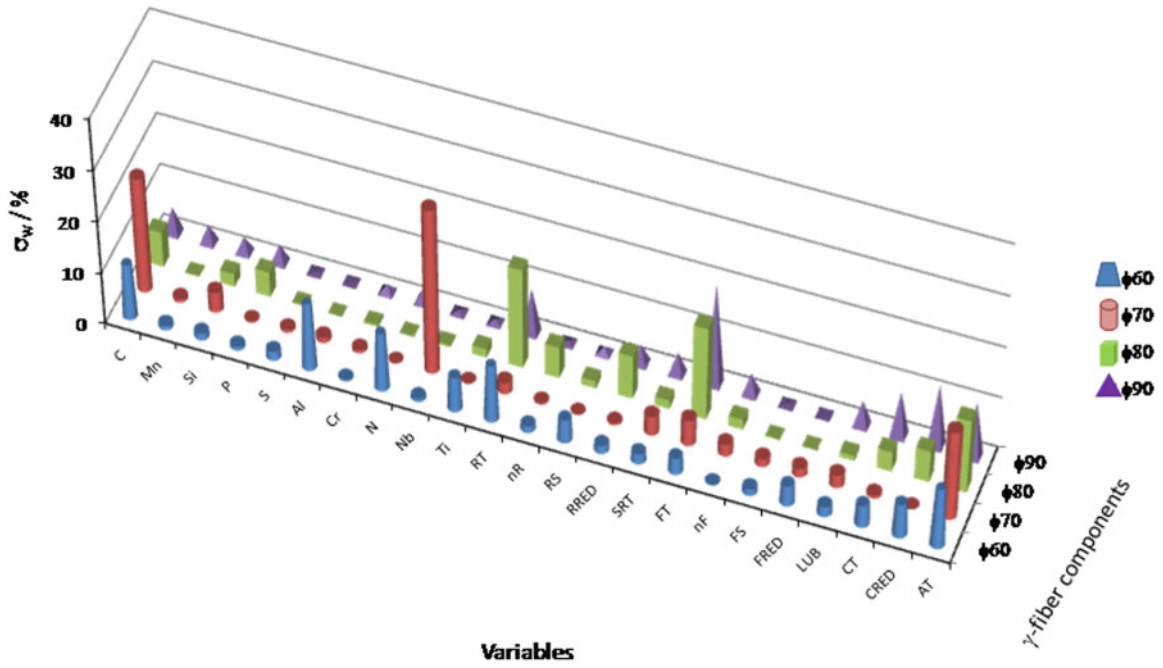

8 Histogram showing significance of input variables in influencing γ-fibre components perceived by their respective best models

relationship expressed by

$$r_m = 0{\cdot}8 + 0{\cdot}6 \log\left[\frac{I(111)}{I(100)}\right] \quad (5)$$

Therefore, the influence of different processing parameters (and chemical composition) on r_m can be evaluated through the $I(111)/I(100)$ ratio by means of the neural network model developed in the present work. Table 5 lists the conditions considered in the calculations. More precisely, two alternative processing routes, which are denoted as 'hot rolling' and 'cold rolling and annealing', have been considered. The former consists of processing the material as it is performed in a traditional hot rolling mill; meanwhile, two additional stages (cold rolling deformation with thickness reduction of 80%) and AT are added to the latter one. Those varying parameters are indicated.

Effect of chemical composition

Figure 12 shows the evolution of r_m for carbon content ranging from 0·002 to 0·02 wt-%. Constant values of Nb and Ti contents (i.e. [Nb]=0·029 wt-% and [Ti]=0·037 wt-%) have been considered. Regarding the processing parameter, fixed values of finishing rolling temperature (FT=930°C), coiling temperature (CT=700°C) and AT (=750°C) have been used in the calculations. The first conclusion that can be drawn from this figure is the significantly higher r_m value for a cold rolled and annealed material as compared with a hot rolled one, which is a consequence of the dramatic texture differences between hot and cold rolled and annealed steels. The recrystallisation of austenite during hot rolling (with FT=930°C) is unimpeded in and is sufficiently rapid to be essentially completed before the transformation to ferrite. This leads to an absence of texture components in ferrite since austenite did not contain any rolling components before transformation.[20] However, the cold rolling process induces stored energy in the material that it is released during subsequent annealing treatment, leading to the formation of deformation free grains

Table 3 Models in committee for each of components of α- and γ-fibres

Fibre component	No. of models in committee	Fibre component	No. of models in committee
Φ0	6	Φ60	3
Φ5	13	Φ65	3
Φ10	12	Φ70	11
Φ15	3	Φ75	1
Φ20	5	Φ80	2
Φ25	4	Φ85	2
Φ30	2	Φ90	9
Φ35	4	ϕ60	1
Φ40	4	ϕ70	2
Φ45	4	ϕ80	3
Φ50	3	ϕ90	2
Φ55	7		

Table 4 Chemical composition (in wt-%) and parameters used to study evolution of hot rolling texture

C/wt-%	0·022
Mn/wt-%	0·14
Si/wt-%	0·071
P/wt-%	0·008
S/wt-%	0·004
Al/wt-%	0·047
Cr/wt-%	0·026
N/wt-%	0·002
Nb/wt-%	0·029
Ti/wt-%	0·037
RT/°C	1050
nR	2
RS/m s^{-1}	0·5
RRED/%	30
SRT/°C	1250/1050
FT/°C	930/800/650
nF	1
FS/m s^{-1}	0·5/7
FRED/%	48
LUB	1

Published by Maney Publishing (c) IOM Communications Ltd

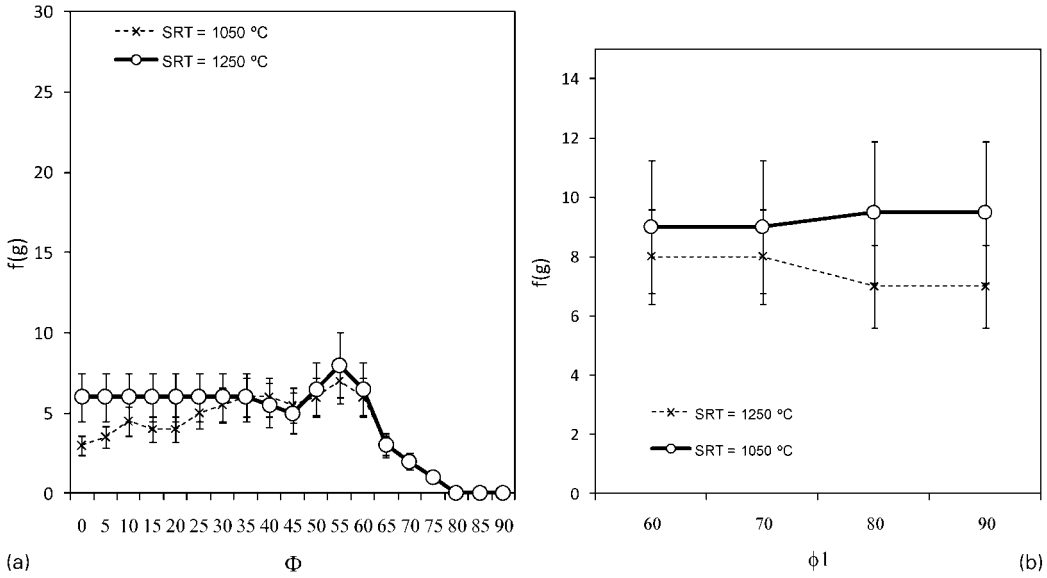

9 Influence of SRT on hot rolling texture *a* α- and *b* γ-fibres

(recrystallisation). On the basis of stored energy considerations, the final texture should be dominated by nuclei, which form soonest and are most numerous. On this basis, the {111} components and a spread of random orientation may be expected, together with a small {110} component, in the cold rolled and annealed steel as compared with a hot rolled steel. This leads to a stronger $I(111)/I(100)$ ratio and hence to a bigger r_m value.

Figure 12 also shows a decrease in r_m as the C content increases for cold rolled and annealed steel. This result is fully consistent with the work reported by Fukuda,[21] where he showed that r_m increased progressively with a decrease in the amount of carbon. These effects have subsequently been corroborated by other workers[22] and confirm the broad idea that high levels of carbon were undesirable in deep drawing quality steels, which can probably be attributed to unfavourable annealing texture components nucleated around the harder second phase pearlite islands.

Figures 13 and 14 show the influence of Ti and Nb additions on the r_m values. The C content in both calculations is kept constant with a value of [C]=0·002 wt-%, FT=930°C, CT=700°C and AT=750°C. It is clear that in both cases the annealed microstructure presents a significant increase in r_m value as the content of both Ti and Nb increases. On the other hand, there is an opposite effect in the hot rolled microstructure. Meanwhile an increase in Ti content raises the value of r_m, an equivalent increase in Nb content induces a drop in r_m value. These results are consistent with the work reported by Hook and co-workers,[23,24] where it was concluded that the austenite in Nb steel is essentially pancaked (unrecrystallised), while the austenite is partially recrystallised in Ti steel. The retardation of austenite recrystallisation in Nb steel during hot rolling is attributable to two complementary factors: the presence of solute Nb in the austenite and the precipitation of Nb carbonitrides in the matrix. Finally, as it is well known,[25,26] the unrecrystallised austenite leads to a finer microstructure after austenite to ferrite transformation, and the finer the microstructure, the lower the $I(111)/I(100)$ ratio,[27] which can explain the decrease in r_m value in Nb bearing steels as compared with Ti steels after the hot rolled stage.

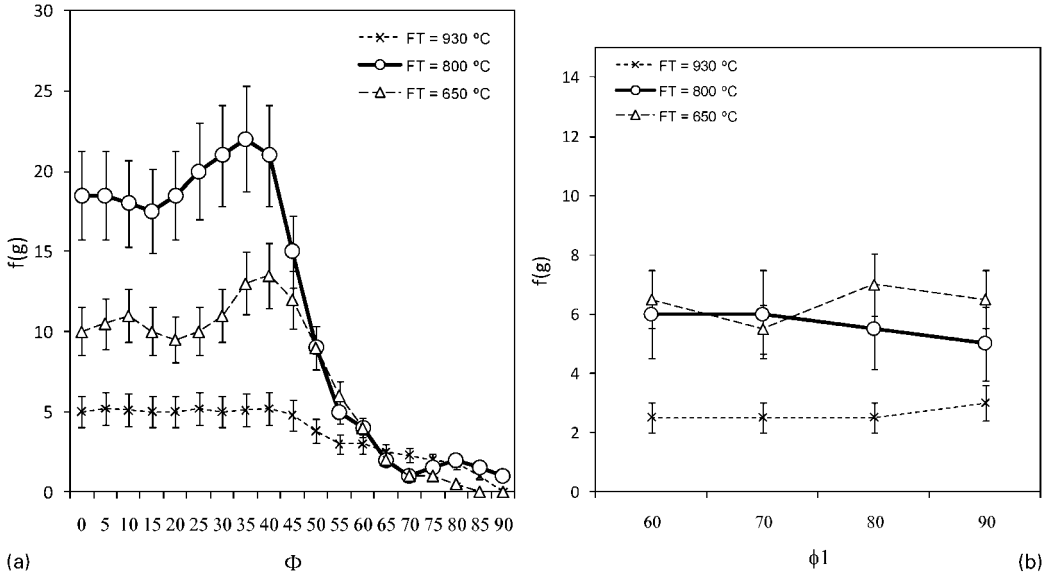

10 Influence of FT on hot rolling texture *a* α- and *b* γ-fibres

Published by Maney Publishing (c) IOM Communications Ltd

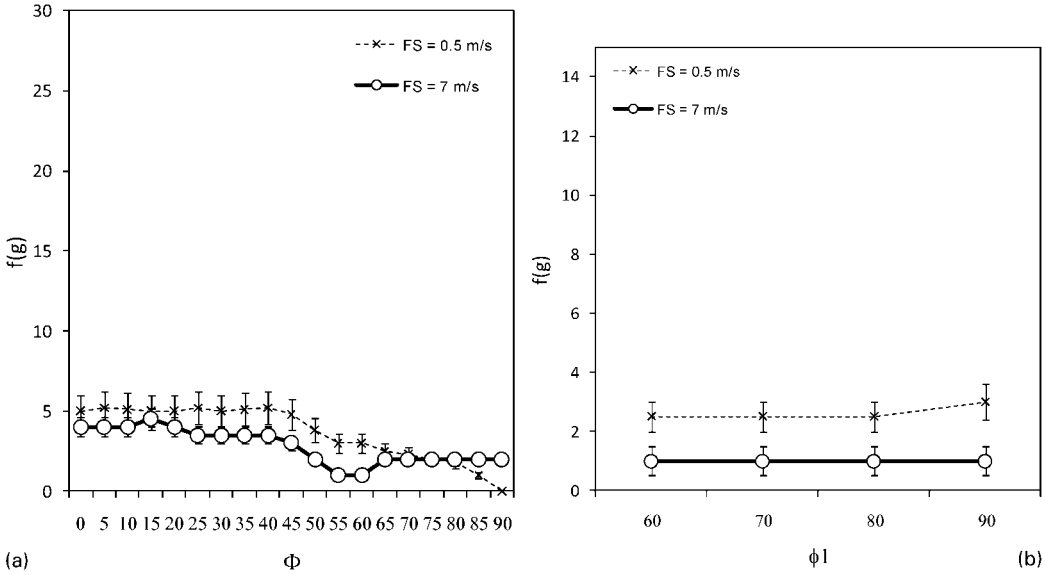

11 Influence of FS on hot rolling texture *a* α- and *b* γ-fibres

Regarding the cold rolled and annealed results, it is clear that both Ti and Nb increase the r_m value. This is because of the very effective role of both Nb and Ti on tiding up the interstitials in the steels. If the carbon in the solid solution is tied up by Nb or Ti, an extensive recovery goes on the γ grains, and the local areas of high concentration of deformation energy quickly become potential nuclei of {111} orientation. This strengthens the γ-fibre, and hence, the $I(111)/I(100)$ ratio increases. However, if the amount of carbon is high (not enough Ti and/or Nb in solid solution), then the recovery is sluggish due to C–Mn dipole immobilising dislocations. In such a case, the grains of lower concentration of deformation energy grow at the expense of the highly deformed {111} grains through a process of stress induced boundary migration. Therefore, the $I(111)/I(100)$ ratio is weak, and hence, r_m decreases.

Effect of processing parameters

The values of C, Ti and Nb considered in the calculation are [C]=0·002 wt-%, [Ti]=0·037 wt-% and [Nb]=0·029 wt-% respectively. A value of coiling temperature of CT=700°C has been considered in the predictions. Figure 15 shows the influence of FT on the r_m value for both hot and cold rolled and annealed materials. It is worth mentioning that the FT values considered here include both austenitic and ferritic rolling. The observed increase in r_m value as FT deceases is related with the fact that, at low FT values, the steel is fully transformed to ferrite. The situation is therefore comparable with the warm ferritic rolling procedure, where rolling takes place in a ferritic stage. Thus, the formation of shear bands occurs, which promotes the formation of dynamically recovered grains of {111} orientation, enhancing the development of a strong γ-fibre texture.[28] This is consistent with the increase in r_m value observed.

Regarding the evolution of cold rolled and annealed material, a more complex behaviour is observed. There is a maximum FT value of 850°C, which is the lowest FT to ensure complete austenitic rolling. In the austenitic rolling

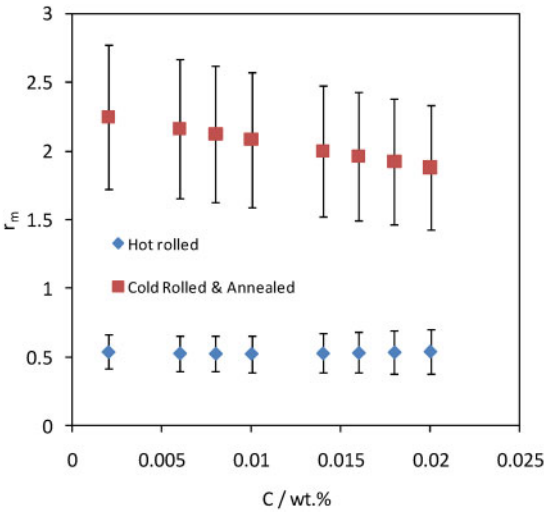

12 Effect of C content on r_m

Table 5 Chemical composition (in wt-%) and parameters used to study evolution of r_m value ('varying' stands for varying conditions of this particular parameter)

	Hot rolled	Cold rolled and annealed
C/wt-%	Varying	Varying
Mn/wt-%	0·14	0·14
Si/wt-%	0·071	0·071
P/wt-%	0·008	0·008
S/wt-%	0·004	0·0026
Al/wt-%	0·047	0·047
Cr/wt-%	0·026	0·026
N/wt-%	0·002	0·002
Nb/wt-%	Varying	Varying
Ti/wt-%	Varying	Varying
RT/°C	1050	1050
nR	2	2
RS/m s^{-1}	0·5	0·5
RRED/%	30	30
SRT/°C	1250	1250
FT/°C	Varying	Varying
nF	1	1
FS/m s^{-1}	0·5	0·5
FRED/%	48	48
LUB	1	1
CT/°C	Varying	Varying
CRED/%	0	80
AT/°C	20	Varying

Published by Maney Publishing (c) IOM Communications Ltd

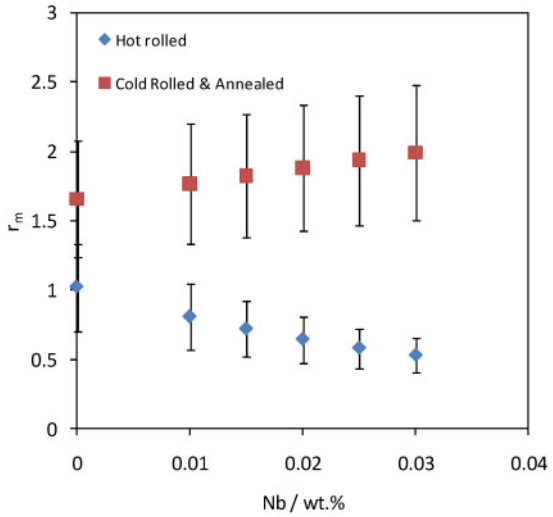

13 Effect of Nb content on r_m

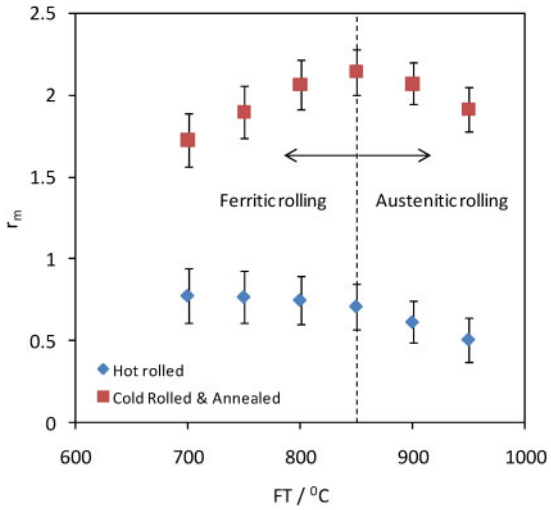

15 Effect of FT temperature on r_m

regime, a lower FT induces an unrecrystallised austenite, which promotes the formation of very fine ferrite grains during the subsequent austenite to ferrite transformation. During annealing after cold rolling, the {111} grains nucleate in the grain boundaries of the deformed ferrite grains. Therefore, the finer the deformed ferrite grain, the more abundant the {111} nucleation events. Thus, the γ-fibre strengthens with the concomitant increase in r_m value. This can explain the increase in r_m when FT is lowered in the austenitic rolling regime.

However, as it was reported by Jeong,[29] the ferrite grain after hot rolling markedly coarsens with a decrease in FT. When the FT is lower than Ar_3, the grain structure just after hot rolling in two phase regions of ferrite and austenite consists of deformed ferrite and deformed austenite grains. The deformed austenite grains immediately transform to strain free ferrite grains, which grow to the surrounding deformed ferrite grains during cooling and coiling simulation at 700°C, leading to the coarse grained structure. The microstructural change with FT in hot rolling is partially responsible for the change in textural evolution during the subsequent cold rolling and annealing, since a cold rolled microstructure still reflects the coarse structure of the hot rolled steel. Therefore, the formation of {111} grains at the grain boundaries of deformed ferrite grains is overcome by a stronger development of the {100} ⟨011⟩ orientation in the annealed sheet, leading to a subsequent decrease in r_m values.

Figure 16 shows the effect of CT on the r_m value. Regarding the hot rolled material, the effect of CT is negligible. Only a slight increase in r_m is observed at low CT values. However, a clear influence on cold rolled and annealed material is observed. This behaviour is consistent with experimental observations,[30,31] where it was reported that final textures are improved by coiling the hot band at high temperature, i.e. above ~700°C. With high temperature coiling, carbide precipitation occurs during very slow cooling of the coiling, and the carbide constituents become coarser and more widely dispersed. Therefore, the ferrite becomes almost completely pure since any residual carbon diffuses to the cementite particles and precipitates out.[32,33] If these carbides are widely spaced and if the steel is heated rapidly after cold rolling, then it is possible for recrystallisation of the ferrite to take place before significant resolution of carbon can occur. The resulting texture contains a strong {111} component and hence a high r_m value.

Figure 17*a* shows the evolution of r_m value with AT after cold rolling (80% reduction in thickness). It could

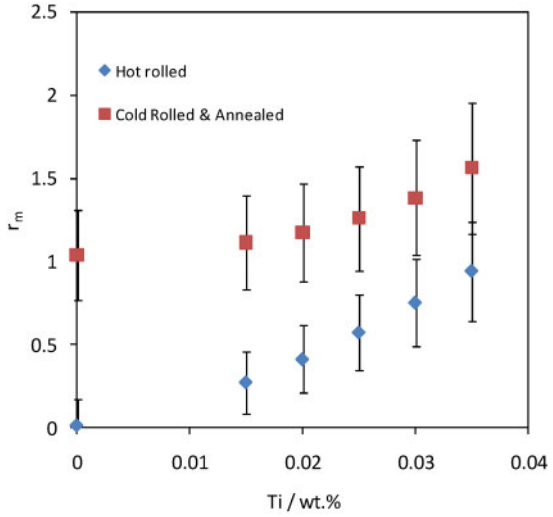

14 Effect of Ti content on r_m

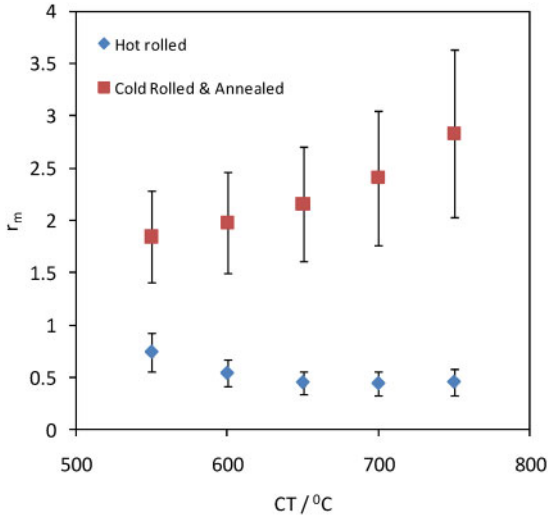

16 Effect of CT temperature on r_m

Published by Maney Publishing (c) IOM Communications Ltd

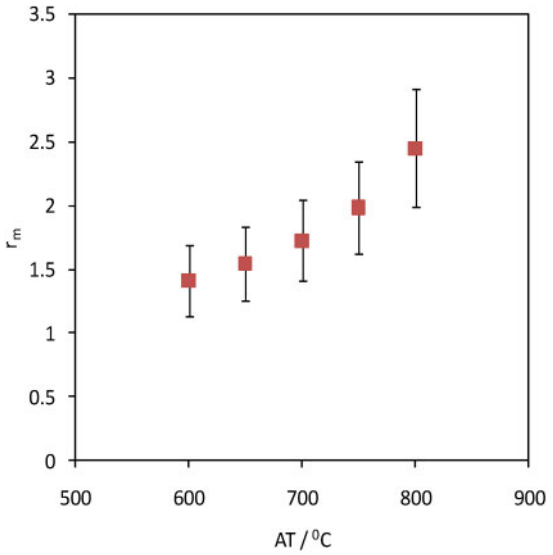

17 Effect of AT temperature on r_m

be concluded from the figure that the higher the AT, the higher the r_m value. This is consistent with the work reported by Petite *et al.*,[27] which demonstrated that there is a linear relationship between the recrystallised grain size and the r_m value. Therefore, the higher the AT, the coarser the grain grows and hence higher values of r_m are achieved.

On the other hand, the carbide dispersion formed during coiling is very important since coarse carbides are very effective on wiping out carbon from ferrite matrix, but the fine dispersion of carbide particles produced by low temperature coiling can release carbon into the matrix during cold rolling by a kind of mechanical dissolution process. According to this view, the dissolved carbon causes dynamic strain aging and leads to inhomogeneous (constrained) deformation in the form of shear bands, which, on subsequent annealing, induce nucleation of unfavourably oriented grains.[34] The fact that carbon can operate in two different ways, i.e. during deformation and during annealing, is highly confusing. In order to clarify this combined effect, Fig. 18 shows the combined influence of CT and AT on the r_m values. It is clear from the figure that the best result in terms of high r_m value is obtained at high CT combined with high AT values, where coarser carbides are formed and

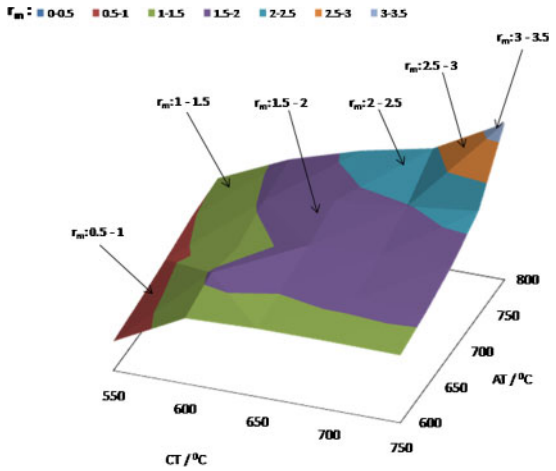

18 Combined effect of CT and AT on r_m value

fast recrystallisation will avoid the nucleation of some unfavourable recrystallised grains around the coarser carbides.[35,36]

Conclusions

A combined neural network under a Bayesian framework has been developed to predict the texture evolution in LC and ELC steels. This model consists of the combination of 23 individual neural network models to deal with the evolution of α- and γ-fibres by varying 23 input parameters describing the chemical composition, and thermomechanical processes, such as austenite and ferrite rolling, coiling, cold working and subsequent annealing, involved on the production route of LC and ELC steels. The predictions of the network within the bounds of the training data set show a good match to the measured values, allowing us to conclude that this combined model is a powerful tool for the fast online prediction of textures in an engineering environment.

The combined neural network model created has been applied to predict the evolution of anisotropy index r_m in DDQ steels with varying chemical composition (C, Ti and Nb content) and processing parameters, such as finishing rolling temperature (FT), coiling temperature (CT) and AT after cold rolling. The results obtained allow us to conclude that cold rolling and annealing processing present a substantially higher r_m value as compared with hot rolling processing.

The model presented in the present paper has been very useful on predicting the influence that C, Ti and Nb in solid solution exert on the r_m value. Higher carbon levels in the solid solution are associated with weaker textures, reducing the r_m value. On the other hand, the Ti and Nb contents substantially increase the r_m value.

The perception of the model to varying values of FT, CT and AT is consistent with measurements reported in literature. Particular attention to the effect of CT and AT has been paid. It has been demonstrated that the r_m value is very sensitive to both parameters. The low CT temperature allows higher amounts of carbon to remain in the solid solution in ferrite and then has a detrimental effect on the r_m values. Meanwhile, a high CT leads to sharper {111} fibre and improved r_m values.

Acknowledgements

The authors acknowledge the financial support from the Spanish Ministerio de Ciencia e Innovación through the Plan Nacional 2009 (grant no. ENE2009 13766-C04-01). The authors are also grateful to Neuromat Ltd for the provision of the neural network software used in the present work.

References

1. B. Hutchinson: *Ironmaking Steelmaking*, 2001, **28**, 145–151.
2. R. Kawalla, W. Jungnickel, H. P. Schmitz, G. Paul, A. de Paepe and W. M. von Haaften: 'Effect of hot and cold rolling technology on textures and plastic anisotropy of flat products', ECSC report, European Commission, Luxembourg, 2007.
3. L. Kestens, I. Gutierrez, J. L. Bocos, J. Zaitegui, V. Cascioli, P E. di Nunzio and R. Grossterlinden: 'Texture control in cold-rolled steel sheets for an optimised arlisotropy', ECSC report, European Commission, Luxembourg, 2002.
4. T. Iung, G. Lannoo, C. G. de Andres and I. Salvatori: 'Metallurgical aspects of the compact reheating treatment of hot-rolled strips before coiling', ECSC report, European Commission, Luxembourg, 2007.

Published by Maney Publishing (c) IOM Communications Ltd

5. C. Capdevila, T. de Cock, C. Garcia-Mateo, F. G. Caballero and C. G. de Andres: *Mater. Sci. Forum*, 2005, **500–501**, 803–810.
6. C. Capdevila, J. P. Ferrer, F. G. Caballero and C. G. de Andres: *Metall. Mater. Trans. A*, 2006, **37A**, 2059–2068.
7. F. G. Caballero, C. Capdevila and C. G. de Andres: *Mater. Sci. Technol.*, 2001, **17**, 1114–1118.
8. C. Capdevila, C. Garcia-Mateo, F. G. Caballero and C. G. de Andres: *Mater. Sci. Technol.*, 2006, **22**, 1163–1170.
9. J. P. Ferrer, T. de Cock, C. Capdevila, F. G. Caballero and C. G. de Andres: *Acta Mater.*, 2007, **55**, 2075–2083.
10. D. J. C. MaKay: *Neural Comput.*, 1992, **4**, 698–705.
11. D. J. C. MaKay: *Darwin College. J.*, 1993, **3**, 81–93.
12. D. J. C. MaKay: *Neural Comput.*, 1992, **4**, 415–422.
13. D. J. C. MaKay: *Neural Comput.* 1992, **4**, 448–460.
14. H. K. D. H. Bhadeshia: *ISIJ Int.*, 1999, **39**, 965–979.
15. Y. Hayakawa and J. A. Szpunar: *Acta Mater.*, 1997, **45**, 4713–4720.
16. W. B. Hutchinson: *Int. Met. Rev.*, 1984, **29**, 25–42.
17. R. K. Ray, J. J. Jonas and R. E. Hook: *Int. Mater. Rev.*, 1994, **39**, 129–172.
18. D. Daniel and J. J. Jonas: *Metall. Trans. A*, 1990, **21A**, 331–342.
19. J. F. Held: 'Mechanical working and steel processing IV'; 1965, New York, The Metallurgical Society of AIME.
20. R. K. Ray and J. J. Jonas: *Int. Mater. Rev.*, 1990, **35**, 1–15.
21. M. Fukuda: *Tetsu-to-Hagane*, 1967, **53**, 559–561.
22. K. Matsudo and T. Shimomura: *Trans. Iron Steel Inst. Jpn*, 1970, **10**, 448–458.
23. R. E. Hook, A. J. Heckler and J. A. Elias: *Metall. Trans. A*, 1975, **6A**, 1683–1672.
24. R. E. Hook and H. Nyo: *Metall. Trans. A*, 1975, **6A**, 1443–1451.
25. A. J. DeArdo: 'Physical metallurgy of interstitial-free steels: precipitates and solutes', 125–136; 2000, Warrendale, PA, International Steel Society (ISS).
26. E. Novillo, M. M. Petite, J. L. Bocos, A. Iza-Mendia and I. Gutierrez: *Adv. Eng. Mater.*, 2003, **5**, 575–578.
27. M. M. Petite, A. Monsalve, I. Gutierrez, J. Zaitegui and J. J. Larburu: *Rev. Metall.*, 1998, **34**, 333–337.
28. A. O. Humphreys, D. Liu, M. R. Toroghinejad, E. Essadiqi and J. J. Jonas: *Mater. Sci. Technol.*, 2003, **19**, 709–714.
29. W. C. Jeong: *Mater. Lett.*, 2008, **62**, 91–94.
30. W. C. Leslie, J. T. Michalak and F. W. Aul: *Texture*, 1978, **3**, 53–72.
31. M. Matsuo, H. Hayakawa and S. Hayami: Proc. 5th Int. Conf. on 'Textures of materials', (ed. G. Gottstein and K. Lücke), 275–284; 1978, Berlin, Springer-Verlag.
32. A. Okamoto and M. Takahashi: Proc. 6th Int. Conf. 'Textures of materials', (ed. S. Nagashima), 739–748; 1981, Tokyo, Iron and Steel Institute of Japan.
33. S. Ono, O. Nozoe, T. Shimomura and K. Matsudo: 'Metallurgy of continuous-annealed sheet steel', (ed. B. L. Bramfitt and P. L Mangonon), 99–115; 1982, Warrendale, PA, The Metallurgical Society of AIME.
34. J. J. Lavigne, T. Suzuki and H. Abe: Proc. 6th Int. Conf. 'Textures of materials', (ed. S. Nagashima), 749–758; 1981, Tokyo, Iron and Steel Institute of Japan.
35. T. de Cock, C. Capdevila, F. G. Caballero and C. G. de Andres: *Mater. Sci. Eng. A*, 2009, **A519**, 9–18.
36. T. de Cock, C. Capdevila, F. G. Caballero and C. G. de Andres: *Mater. Trans.*, 2008, **49**, 2292–2297.

Published by Maney Publishing (c) IOM Communications Ltd

View publication stats